Commun. Math. Res.
doi: 10.4208/cmr.2026-0017

Vol. **x**, No. x, pp. 1-18
x 2026

A High-Order Oscillation-Free Discontinuous Galerkin Scheme for One-Dimensional Compressible Multi-Material Flows

Xiangyuan Li[1], Zhenzhen Li[2], Xijun Yu[3], Xiaolong Zhao[1,*] and Fang Qing[4]

[1] *School of Mathematics and Statistics, Zhengzhou University, Zhengzhou 450001, P.R. China.*
[2] *College of Mathematics and Information Science, Zhengzhou University of Light Industry, Zhengzhou 450002, P.R. China.*
[3] *Laboratory of Computational Physics, Institute of Applied Physics and Computational Mathematics, Beijing 100088, P.R. China.*
[4] *School of Mathematics and Statistics, Hunan First Normal University, Changsha 410205, China.*

Received 29 January 2026; Accepted 31 March 2026

Abstract. In this paper, a high-order oscillation-free (OF) discontinuous Galerkin (DG) scheme is presented for one-dimensional compressible multi-material flows. For describing the dynamics of fluid mixture, we couple a conservative equation related to the volume-fraction model with the Euler equations. For controlling the oscillations, some damping terms are added into the weak formulation of the system to automatically adjust the high-order terms. There are not any parameters which need to be adjusted artificially in the new damping terms, and the difficulties in solving discontinuous solutions and complexities of designing limiters can be avoided. Our scheme can be applied to the simulation of compressible multi-material flows efficiently with the essentially non-oscillatory property. Moreover, our scheme can be extended to the one with any high order as long as the order of basis functions is increased. In this paper, we only study the third-order OFDG scheme with the basis functions

*Corresponding author. *Email addresses:* yuan0418@stu.zzu.edu.cn (X. Li), lyzhenzhen86@163.com (Z. Li), yuxj@iapcm.ac.cn (X. Yu), xiaolongzhao109@zzu.edu.cn (X. Zhao), qingfang46@126.com (F. Qing)

up to the quadratic polynomial. Some examples are tested to demonstrate the third-order accuracy and essentially non-oscillatory property of our scheme.

AMS subject classifications: 65M60, 76N15, 76M25

Key words: Compressible multi-material flows, oscillation-free DG scheme, damping terms, volume-fraction model, essentially non-oscillatory property.

1 Introduction

The hydrodynamics of multi-material flows is of great interest in computational fluid dynamics (CFD) and exists in many problems. It has wide application in the fields of national economy and energy, etc. The simulation of compressible multi-material flows has the great theoretic significance and application value for understanding the physical phenomena in nuclear physics, biological engineering and many other research fields. So, the research for the numerical simulations of compressible multi-material flows has obtained more and more attention from the scholars in recent years. Some difficulties such as the numerical oscillations may arise at material interfaces in the implementations of the conservative methods for multi-material flows. In recent decades, significant progress has been obtained in the development of the numerical schemes for simulating multi-material flows, one can see e.g. [1–3,12,13]. Abgrall and Karni [2] reviewed some numerical algorithms which were proposed, and they pointed the common key ideas of these algorithms. Among these schemes, an extended system including the Euler equations has been studied in which additional equations were used to describe the evolutions of fluid parameters such as the volume-fraction, level set function or ratio of specific heats of fluid mixture. For maintaining the pressure equilibrium and eliminating the spurious oscillations near the regions involving material interfaces, many scholars have studied various models (e.g. the volume-fraction model, etc.), and they have proposed several schemes with an additional non-conservative equation for describing fluid mixture, one can see e.g. [2]. In this work, we will construct a conservative scheme combined with an additional conservative equation for multi-material flows, and a volume-fraction model [4,19,25] which belongs to the diffusion interface models will be chosen to obtain the equation of state (EOS) of fluid mixture.

As we know, the DG method has been widely used for handling various models in many fields, e.g. compressible flows involving complex geometries and discontinuities. In the DG method, the solution of the model is approximated with the help of basis functions in each cell, which leads to a direct piecewise

high-order representation of the solution. Liu *et al.* [22] developed a high-order DG method for solving the incompressible Navier-Stokes equations. Boscheri *et al.* [5] proposed a high-order accurate nodal DG method for the solution of nonlinear hyperbolic systems of partial differential equations on unstructured polygonal Voronoi meshes. Xia *et al.* [23] established a high-order accurate DG method for the compressible Euler equations under gravitational fields on unstructured meshes.

Due to the nonlinearity of hyperbolic equations, their solution may evolve into discontinuities. The generated spurious oscillations near the discontinuities may make the scheme less robust and seriously affect the accuracy of numerical results. For controlling the spurious oscillations near the discontinuities in the DG methods, many kinds of slope limiters have been developed such as the total variation diminishing (TVD) limiter, total variation bounded (TVB) limiter and weighted essentially non-oscillatory (WENO) limiter and so on, see e.g. [18, 26] for more details. After we have obtained the numerical solutions of DG methods, the slope limiting process will be applied into the modification of numerical solutions. The limiters often involve some problem-dependent parameters. With suitable adjustments of these parameters, the schemes may work well and then obtain satisfactory results. Another kind of approach is introducing artificial terms such as the artificial diffusion directly in the weak formulation so as to obtain certain properties such as entropy stability, see e.g. [11] for more details. However, the artificial diffusion may also involve some problem-dependent parameters. If these parameters are not adjusted properly, the resolution of numerical solution near the shocks may be smeared, or some visible spurious oscillations will be caused near the discontinuities. Lu [16] proposed a new approach to control spurious oscillations in the DG schemes for scalar hyperbolic conservation laws. Based on the classical DG method, the scheme introduces a damping term with the local L_2 projection to adjust the high-order terms. Using a unified choice of the damping parameters, the new damping term is small when the numerical solution keeps smooth, and it is large enough near the discontinuities. Without any parameters which need to be adjusted, this new damping term can automatically detect the intensity of discontinuities and control the spurious oscillations near the strong discontinuities. The proposed oscillation-free discontinuous Galerkin (OFDG) scheme can maintain many good properties such as conservation and so on. Numerical examples verified that the proposed OFDG method controlled the spurious numerical oscillations effectively without affecting the accuracy. Liu [15] extended the OFDG method to the hyperbolic conservation laws and constructed the damping terms involving the characteristic variables. Without any limiters or artificial diffusion, several tough numerical tests such as

the high Mach number astrophysical jets problem showed that the OFDG scheme controlled the spurious numerical oscillations effectively, which demonstrated the effectiveness of proposed scheme. Liu *et al.* [9] developed an OFDG method for solving the multi-component chemically reacting flows, and the reactive Euler equations and Navier-Stokes equations are considered. In addition, Zuo *et al.* [27] added the artificial damping terms into the simulation of the reactive Euler equations, and they proposed a positivity preserving and oscillation-free entropy stable discontinuous Galerkin scheme for the reactive Euler equations. Tao [20] developed an oscillation-free local discontinuous Galerkin (OFLDG) method for solving nonlinear degenerate parabolic equations. Some numerical experiments demonstrated that the proposed method controlled the spurious oscillations well and maintained the high-order accuracy of the scheme. Recently, some scholars developed several variants of the oscillation-free DG method, such as the oscillation-eliminating DG proposed by Wu *et al.* [17] and jump filter methods proposed by Xia *et al.* [28], which have the unique characteristics and advantages. One can see [17,28] for more details.

Taking into account the advantages of the OFDG method, we will develop a high-efficiency and concise OFDG scheme for one-dimensional compressible multi-material flows in the present work. Considering the complexity of some slope limiters such as the Hermite weighted essential non-oscillatory (HWENO) reconstruction and so on in the high-order DG schemes, the global damping terms for all components are added into the weak formulation of multi-material system in this work to control the spurious oscillations, and any extra limiter is no more mandatory. There are not any problem-dependent parameters which need to be adjusted, which can greatly improve the simplicity of scheme. Moreover, we couple the compressible Euler equations with a conservative equation associated with the volume-fraction to describe fluid flows, which is a new attempt for the simulation of multi-material flows by the OFDG method. It is also worth noting that our scheme only applies to two-material flows involving the compressible ideal gases in one-dimensional geometry at present, and we will extend the application of this scheme to wider fields in the future work. The performance of our multi-material OFDG scheme is verified by solving compressible flows. It is observed that the proposed multi-material OFDG scheme can resolve sharp flow structures and essentially prevent the occurrence of spurious oscillations. Due to its relative simple formulation, our scheme is a possible alternative oscillation-free scheme for the simulations of multi-material flows involving strong discontinuities.

The outline of the rest of this paper is organized as follows. In Section 2, the governing equations and individual steps of simulating one-dimensional com-

pressible multi-material flows by our OFDG scheme are shown. In Section 3, some examples are used to assess the good properties of our scheme. Finally, some concluding remarks for this work are shown in Section 4.

2 The oscillation-free DG scheme for compressible multi-material flows

2.1 Governing equations

The Euler equations for one-dimensional inviscid compressible flows can be expressed as follows:

$$\begin{cases} \dfrac{\partial \rho}{\partial t}+\nabla\cdot(\rho u)=0, \\ \dfrac{\partial(\rho u)}{\partial t}+\nabla\cdot(\rho u^2+p)=0, \\ \dfrac{\partial(\rho E)}{\partial t}+\nabla\cdot(\rho E u+pu)=0, \end{cases} \tag{2.1}$$

where t is time instant, ρ is density, u is velocity, p is pressure, E denotes specific total energy, and $\mathscr{E}=E-u^2/2$ denotes specific internal energy.

In this work, our interest is centered on the perfect gases. The Euler equations are closed by an additional equation of state for the perfect gases which can be described as the following EOS:

$$p=(\gamma-1)\rho\mathscr{E},$$

where γ denotes the effective ratio of specific heats of fluid mixture. A variable Φ will be chosen to describe the dynamics of fluid mixture, and we use a conservative equation of Φ

$$\frac{\partial(\rho\Phi)}{\partial t}+\nabla\cdot(\rho\Phi u)=0 \tag{2.2}$$

to obtain the EOS of fluid mixture. Some choices of Φ which depend on the model assumptions have been studied in other literatures. For example, Φ can be set to the effective ratio of specific heats or the volume-fraction, etc. In this work, the interface of two materials with different γ will be considered as a contact discontinuity of γ, we will use the volume-fraction model [4, 19, 25] with the volume-fraction Φ to describe the fluid compositions and obtain effective EOS of fluid mixture. To close the system, we will adopt the isobaric assumption in [4]. That is, all fluid pressures are equal in a cell. This work employs the multi-material

volume fraction model, grounded in local mechanical and thermodynamic equilibrium, with the pressure continuity assumption satisfied at the interface. This assumption strictly adheres to the Rankine-Hugoniot discontinuity conditions in strong discontinuous flows involving shock waves, and it is physically rigorous and reasonable. Numerically, the single pressure field can be directly coupled with classical Riemann solvers such as HLL and HLLC, effectively suppressing pressure oscillations and non-physical diffusion during the interaction between shock waves and interfaces, thus ensuring the robustness and convergence of the algorithm under strong discontinuities. Therefore, the isobaric assumption is a self-consistent and necessary closure condition in compressible multi-material simulations with volume-fraction model. The EOS of fluid mixture can be expressed by

$$p=(\overline{\gamma}-1)\rho\mathscr{E}. \tag{2.3}$$

The average specific heat ratio $\overline{\gamma}$ of fluid mixture is obtained by

$$\frac{1}{\overline{\gamma}-1}=\frac{\Phi_1}{\gamma_1-1}+\frac{\Phi_2}{\gamma_2-1},$$

where $\Phi_1=\Phi$ (or $\Phi_2=(1-\Phi)$) denotes the volume-fraction of composition '1' (or composition '2'), γ_1 (or γ_2) denotes the specific heat ratio of composition '1' (or composition '2').

The conservative Eq. (2.2) can be coupled with the Euler equations as follows:

$$\begin{cases}\dfrac{\partial\rho}{\partial t}+\nabla\cdot(\rho u)=0,\\ \dfrac{\partial(\rho u)}{\partial t}+\nabla\cdot(\rho u^2+p)=0,\\ \dfrac{\partial(\rho E)}{\partial t}+\nabla\cdot(\rho Eu+pu)=0,\\ \dfrac{\partial(\rho\Phi)}{\partial t}+\nabla\cdot(\rho\Phi u)=0.\end{cases} \tag{2.4}$$

For the sake of clarity, we define $\mathbf{U}=(\rho,\rho u,\rho E,\rho\Phi)^T$. For obtaining the EOS of fluid mixture and accomplishing the simulation of flow field, we will design our algorithm as the following steps:

Step 1. Define the initial value of volume-fraction Φ. We set the initial value

$$\Phi=(\Phi_1)_{t=0}=1,\quad (\Phi_2)_{t=0}=(1-\Phi_1)_{t=0}$$

for fluid composition '1', and set

$$\Phi=(\Phi_2)_{t=0}=1,\quad (\Phi_1)_{t=0}=(1-\Phi_2)_{t=0}$$

for fluid composition '2'.

Step 2. At a certain time step, we obtain $(\rho\Phi)$ and ρ of fluid mixture by solving Eqs. (2.4). Then, Φ is locally computed from the quotient $\Phi=(\rho\Phi)/\rho$, meanwhile we can obtain $\Phi_1=\Phi$ and $\Phi_2=1-\Phi_1$.

Step 3. With the isobaric assumption, we acquire the $\overline{\gamma}$ of fluid mixture at this time step.

Step 4. With $\overline{\gamma}$ and the uniform EOS (2.3), we implement the numerical simulation at the next time step.

2.2 Spatial discretization and time discretization

The space discretization will be accomplished by the DG method in this paper. The domain is set to Ω which is filled by the inviscid fluid, and we discretize the domain into a set of non-overlapping cells $\{\mathscr{D}_i \,|\, i=1,\ldots,M\}$ whose reunion covers Ω. $\mathscr{D}_i:=\{x \,|\, x_i\le x\le x_{i+1}\}$ denotes the i-th cell with two nodes x_i and x_{i+1}.

Firstly, we will introduce the following weak formulation of Eqs. (2.4). For any test function $\varphi(x)\in L^2(\Omega)$, we multiply both sides of (2.4) by $\varphi(x)$ and integrate them on Ω to get the following form:

$$\begin{cases}\displaystyle\int_\Omega \frac{\partial\rho}{\partial t}\varphi d\Omega+\int_\Omega \nabla\cdot(\rho u)\varphi d\Omega=0,\\ \displaystyle\int_\Omega \frac{\partial(\rho u)}{\partial t}\varphi d\Omega+\int_\Omega \nabla\cdot(\rho u^2+p)\varphi d\Omega=0,\\ \displaystyle\int_\Omega \frac{\partial(\rho E)}{\partial t}\varphi d\Omega+\int_\Omega \nabla\cdot(\rho Eu+pu)\varphi d\Omega=0,\\ \displaystyle\int_\Omega \frac{\partial(\rho\Phi)}{\partial t}\varphi d\Omega+\int_\Omega \nabla\cdot(\rho\Phi u)\varphi d\Omega=0.\end{cases}\tag{2.5}$$

Secondly, we define the finite-element space as the following set of piecewise polynomials:

$$V_h^k=\Big\{\varphi_h\in L^2(\Omega):\ \varphi_h\,|_{\mathscr{D}_i}\in P^k(\mathscr{D}_i);\ 1\le i\le M\Big\},$$

where $P^k(\mathscr{D}_i)$ denotes a set of polynomials of degree up to k defined in $\mathscr{D}_i$. For all

test functions $\varphi_h \in V_h^k$ and all cells $\mathscr{D}_i$, we should find the approximate function $\mathbf{U}_h=(\rho_h,(\rho u)_h,(\rho E)_h,(\rho\Phi)_h)^T \in V_h^k$ that satisfies

$$\begin{cases} \int_{\mathscr{D}_i} \dfrac{\partial \rho_h}{\partial t}\varphi_h d\mathscr{D}_i + \int_{\mathscr{D}_i} \nabla\cdot(\rho u)_h \varphi_h d\mathscr{D}_i = 0, \\ \int_{\mathscr{D}_i} \dfrac{\partial (\rho u)_h}{\partial t}\varphi_h d\mathscr{D}_i + \int_{\mathscr{D}_i} \left(\nabla\cdot(\rho u^2)_h + \nabla\cdot p_h\right)\varphi_h d\mathscr{D}_i = 0, \\ \int_{\mathscr{D}_i} \dfrac{\partial (\rho E)_h}{\partial t}\varphi_h d\mathscr{D}_i + \int_{\mathscr{D}_i} \nabla\cdot\left((\rho E u)_h + (pu)_h\right)\varphi_h d\mathscr{D}_i = 0, \\ \int_{\mathscr{D}_i} \dfrac{\partial (\rho\Phi)_h}{\partial t}\varphi_h d\mathscr{D}_i + \int_{\mathscr{D}_i} \nabla\cdot(\rho\Phi u)_h \varphi_h d\mathscr{D}_i = 0. \end{cases} \tag{2.6}$$

Using the divergence theorem, Eqs. (2.6) can be equivalently reformulated as

$$\frac{d}{dt}\int_{\mathscr{D}_i} \mathbf{U}_h \varphi_h d\mathscr{D}_i = R_i(\mathbf{U}_h), \tag{2.7}$$

where

$$R_i(\mathbf{U}_h) = \int_{\mathscr{D}_i} F(\mathbf{U}_h)\partial_x\varphi_h d\mathscr{D}_i - \left(\widehat{F_{i+1}(\mathbf{U}_h)}\varphi_h(x_{i+1}) - \widehat{F_i(\mathbf{U}_h)}\varphi_h(x_i)\right),$$

$$F(\mathbf{U}_h) = \begin{pmatrix} F_1 \\ F_2 \\ F_3 \\ F_4 \end{pmatrix} = \begin{pmatrix} (\rho u)_h \\ (\rho u^2)_h + p_h \\ (\rho E u)_h + (pu)_h \\ (\rho\Phi u)_h \end{pmatrix},$$

and $\widehat{F_i(\mathbf{U}_h)}$ denotes the numerical flux at the boundary x_i of cell $\mathscr{D}_i$. In this work, the Harten-Lax-van Leer contact wave (HLLC) flux is chosen as the replacement of numerical flux $\widehat{F_i(\mathbf{U}_h)}$. Without the extra damping terms, the scheme Eq. (2.7) is exactly a standard DG scheme and it may generate some spurious oscillations near the discontinuities. Following [15], adding the numerical damping terms, the semi-discrete OFDG scheme for Eqs. (2.1) is obtained with the following form:

$$\frac{d}{dt}\int_{\mathscr{D}_i} \mathbf{U}_h \varphi_h d\mathscr{D}_i = R_i(\mathbf{U}_h) - \sum_{l=0}^{k} \frac{\sigma_i^l}{\Delta\mathscr{D}_i}\int_{\mathscr{D}_i}\left(\mathbf{U}_h - P_h^{l-1}\mathbf{U}_h\right)\varphi_h d\mathscr{D}_i, \tag{2.8}$$

where $\Delta\mathscr{D}_i = x_{i+1} - x_i$, P_h^l with $0 \le l \le k$ is the standard L_2 projection that for any vector function $\boldsymbol{\omega}$, $P_h^l\boldsymbol{\omega} \in V_h^l$ satisfies

$$\int_{\mathscr{D}_i}\left(P_h^l\boldsymbol{\omega} - \boldsymbol{\omega}\right)\varphi_h d\mathscr{D}_i = 0, \tag{2.9}$$

$$V_h^l=\left\{\varphi_h\in L^2(\Omega):\ \varphi_h\,|_{\mathscr{D}_i}\in P^l(\mathscr{D}_i);\ 1\le i\le M\right\}.$$

In particular, here we define $P_h^{-1}=P_h^0$. The key idea for constructing the damping coefficients is to ensure they become large near the discontinuities and are small in the smooth regions. A natural approach is to use the jumps of adjacent cells. Therefore, we will construct the damping coefficients by using the jumps of numerical solution at the cell interfaces, and we define them as follows:

$$\sigma_i^l=\frac{2(2l+1)}{(2k-1)}\frac{h^l}{l!}\max_{1\le s\le 4}\left(\left([\partial_x^l W_s]_i\right)^2+\left([\partial_x^l W_s]_{i+1}\right)^2\right)^{\frac{1}{2}},\tag{2.10}$$

where $[\partial_x^l W_s]_i=w(x_i^+)-w(x_i^-)$ denotes the jump of variable w at the node x_i, w represents any component of $\mathbf{U}=(\rho,\rho\mathbf{V},\rho E,\rho\Phi)^T$ and $h=\max_{\{i=1,\dots,M\}}\{\Delta\mathscr{D}_i\}$. The variable $\partial_x^l\boldsymbol{W}=(\partial_x^l W_1,\cdots,\partial_x^l W_4)^T$ is given by $\partial_x^l\boldsymbol{W}=\boldsymbol{R}^{-1}\partial_x^l\boldsymbol{U}_h$ at x_i, where $\boldsymbol{R}^{-1}$ is the matrix derived from the characteristic decomposition $F'(\overline{(\boldsymbol{U}_h)_i})=\boldsymbol{R}\boldsymbol{\Lambda}\boldsymbol{R}^{-1}$, and $\overline{(\cdot)}_i$ stands for the arithmetic mean value of the variable which will be used in the numerical experiments later. Obviously, the formulation of damping coefficients is not unique, and its main purpose is to control the spurious oscillations. Thus, for providing sufficiently large damping term for the DG scheme near the discontinuity and then achieving the desired oscillation-free effect, using the maximum of two neighboring jumps is a robust choice. Specially, taking $\varphi_h=1$ and with (2.8), we can obtain

$$\begin{aligned}\frac{d}{dt}\int_{\mathscr{D}_i}\mathbf{U}_h d\mathscr{D}_i&=-\widehat{F_{i+1}(\mathbf{U}_h)}+\widehat{F_i(\mathbf{U}_h)}-\sum_{l=0}^{k}\frac{\sigma_i^l}{\Delta\mathscr{D}_i}\int_{\mathscr{D}_i}\left(\mathbf{U}_h-P_h^{l-1}\mathbf{U}_h\right)d\mathscr{D}_i\\&=-\widehat{F_{i+1}(\mathbf{U}_h)}+\widehat{F_i(\mathbf{U}_h)}.\end{aligned}\tag{2.11}$$

Summing it over all $\mathscr{D}_i$, we can obtain that

$$\frac{d}{dt}\int_\Omega\mathbf{U}_h dx=0,\tag{2.12}$$

which shows the conservation of $\mathbf{U}_h$.

Next, setting $x_{i+1/2}=(x_i+x_{i+1})/2$, the Taylor's basis functions for $P^2(\mathscr{D}_i)$

$$\psi_{i1}(x)=1,\quad \psi_{i2}(x)=\frac{2(x-x_{i+1/2})}{\Delta\mathscr{D}_i},\quad \psi_{i3}(x)=\left(\psi_{i2}^2(x)-\frac{1}{3}\right)$$

are chosen as a set of basis functions of V_h^k, and

$$(\mathbf{U}_h)_i(x)=\sum_{r=1}^{3}(\widehat{\mathbf{U}}_h)_{ir}\psi_{ir},\quad x\in\mathscr{D}_i,\tag{2.13}$$

where

$$(\widehat{\mathbf{U}}_h)_{ir}=\left[(\rho_h)_{ir},((\rho u)_h)_{ir},((\rho E)_h)_{ir},((\rho\Phi)_h)_{ir}\right]^T.$$

Since Eqs. (2.8) are satisfied for all test functions, we choose ψ_m $(m=1,2,3)$ as the test function φ_h.

Finally, we set

$$\mathbf{M}_i=\int_{\mathscr{D}_i}\psi_{ir}\psi_{im}d\mathscr{D}_i,\quad r,m=1,2,3, \tag{2.14}$$

Eqs. (2.8) will become to

$$\frac{d}{dt}\mathbf{M}_i\cdot[(\widehat{\mathbf{U}}_h)_{i1},(\widehat{\mathbf{U}}_h)_{i2},(\widehat{\mathbf{U}}_h)_{i3}]=L_i(\mathbf{U}_h), \tag{2.15}$$

where

$$L_i(\mathbf{U}_h)=R_i(\mathbf{U}_h)-\sum_{l=0}^{k}\frac{\sigma_i^l}{\Delta\mathscr{D}_i}\int_{\mathscr{D}_i}(\mathbf{U}_h-P_h^{l-1}\mathbf{U}_h)\varphi_h d\mathscr{D}_i.$$

Moreover, we use the explicit third-order TVD Runge-Kutta method [7,8] to implement time discretization of Eqs. (2.15). The time steplength at the n-th time step is

$$(\Delta t)^n=\lambda\cdot\min_{i=1,\ldots,M}\left(\frac{1}{((c_i^n+|u_i^n|)/h)+a_0/h}\right), \tag{2.16}$$

where c_i^n is the sound speed at the centroid of $\mathscr{D}_i$ and u_i^n is the value of u at the centroid of $\mathscr{D}_i$, and $a_0=\max_{\{i=1,2,\ldots,M\}}\Sigma_{l=0}^k\sigma_i^l$, σ_i^l is the damping coefficient for $\mathscr{D}_i$ in the scheme. The term a_0 acts as an additional artificial viscosity that restricts the time step. For the sake of stability, the Courant number λ of the ordinary RKDG scheme with P^2 should satisfy this condition: $\lambda\leq 1/3$, which is detailed in [7,8]. The time step size of our OFDG scheme could be more restricted than the one of ordinary RKDG scheme, and we simulate the following tests with $\lambda=0.1$.

3 Numerical examples

In this section, several examples are presented to demonstrate the accuracy and the good performances of our scheme. If there is no special explanation, all the boundary conditions will be the wall boundary conditions.

3.1 The single-material problems

3.1.1 The accuracy test

This example is a smooth problem [6] for testing the accuracy of our scheme. The initial condition is set to

$$\rho_0 = 2+\sin(2\pi x), \quad p_0 = 1, \quad u_0 = 1+0.1\sin(2\pi x)$$

in the domain $x \in [0,1]$, and the test time is set to $t = 0.1$. The numerical solution obtained by our scheme in the Eulerian manner on 8000 fixed cells is chosen as the reference solution. In this example, the errors are set to the arithmetical average values of the integral average errors in all cells. The L^1, L^2, L^∞ errors and convergence orders of our scheme for density ρ are shown in Table 1. It can be seen that the convergence rates are excellent and clearly demonstrate third-order accuracy of our scheme.

Table 1: The errors for density of the smooth problem.

Cells	L^1 error	Order	L^2 error	Order	L^∞ error	Order
40	1.2308E-005	–	1.7185E-005	–	6.7159E-005	–
80	1.7402E-006	2.8223	2.4256E-006	2.8247	9.7238E-006	2.7880
160	2.4179E-007	2.8474	3.3096E-007	2.8736	1.3146E-006	2.8869
320	3.1682E-008	2.9320	4.3578E-008	2.9250	1.7584E-007	2.9023

3.1.2 The Sod's shock tube problem

The second example which we will test is the Sod's shock tube problem [14]. In this example, we will evaluate the ability to capture each kind of wave and the essentially non-oscillatory property of our scheme. The computational domain of this case is $[0,1]$ with 200 mesh cells, the initial condition is as follows:

$$(\rho,u,p,\gamma) = \begin{cases} (1.0,0,1.0,1.4), & \text{if} \quad x \le 0.5, \\ (0.125,0,0.1,1.4), & \text{otherwise}, \end{cases}$$

and the final time is $t = 0.2$. Fig. 1 shows the distributions of density and pressure obtained by our OFDG scheme. The comparison between the exact solution and our result shows that our numerical solution approximates the exact one well and our scheme has essentially non-oscillatory property.

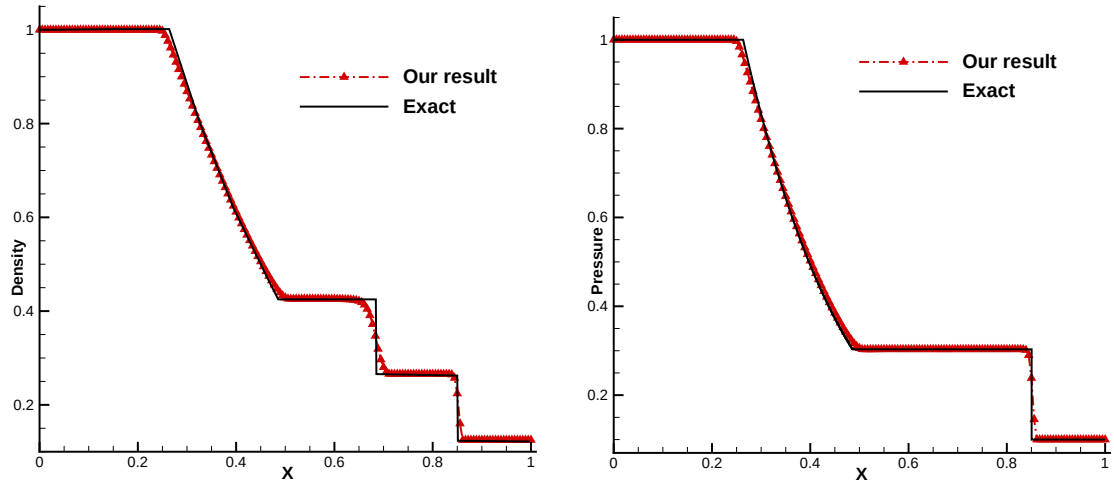

(a) Density (b) Pressure

Figure 1: The result of Sod's shock tube problem.

3.1.3 The interaction of two blast waves

The final single-material example which we will test is the interaction of two blast waves [6, 21]. The computational domain of this example is set to $[0,1]$, and the initial condition is

$$(\rho,u,p,\gamma)=\begin{cases}(1.0,1.0,1000,1.4), & \text{if} \quad 0<x<0.1,\\ (1.0,1.0,0.01,1.4), & \text{if} \quad 0.1<x<0.9,\\ (1.0,1.0,100,1.4), & \text{if} \quad 0.9<x<1.0.\end{cases}$$

The final time is $t=0.038$, and the reflective boundary condition is imposed on both left and right boundaries. The reference solution is computed by a third-order DG scheme with 4000 cells.

Fig. 2 shows the distribution of density with 400 cells and a local zoomed-in drawing of the distribution of density. The comparison between the reference solution and our result shows that the numerical solution with the non-oscillatory property approximates the reference one, which verifies the performance of our scheme for the complex wave interaction.

3.2 The multi-material problems

3.2.1 A multi-material shock tube problem

This example is a multi-material shock tube problem. In this example, the computational domain is $[0,20]$, the initial condition of this example is as follows:

$$(\rho,u,p,\gamma)=\begin{cases}(1.0,0,500.0,1.4), & \text{if} \quad x\leq 10.0,\\ (1.0,0,0.2,1.6), & \text{otherwise},\end{cases}$$

and the final time is $t=0.2$. Fig. 3 shows the distributions of density and pressure. Through the comparison between the exact solution and our result with 400 cells, we can see that our numerical solution approximates the exact one well and has good non-oscillatory property, which indicates our algorithm with robustness can essentially reduce the spurious oscillations.

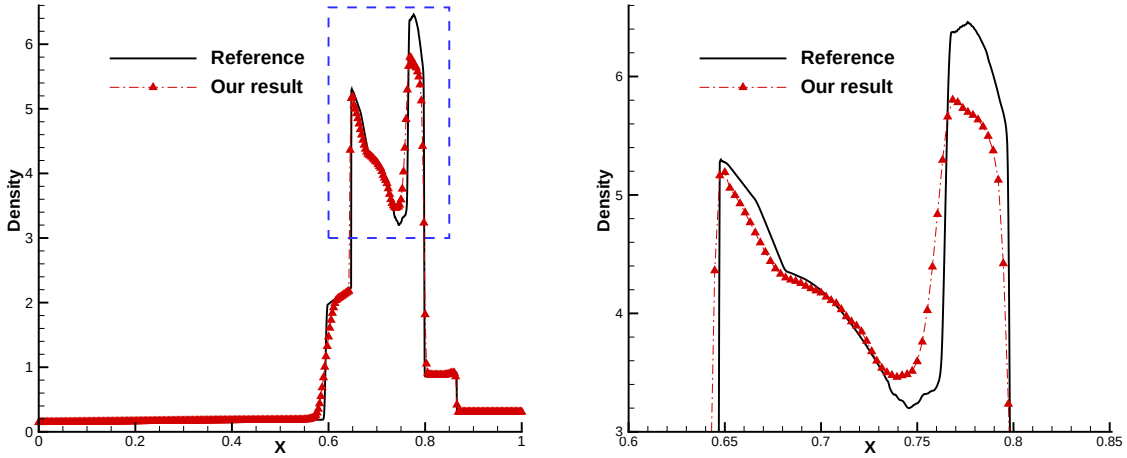

(a) Density (b) Local zoomed-in drawing of density

Figure 2: The result of interaction of two blast waves.

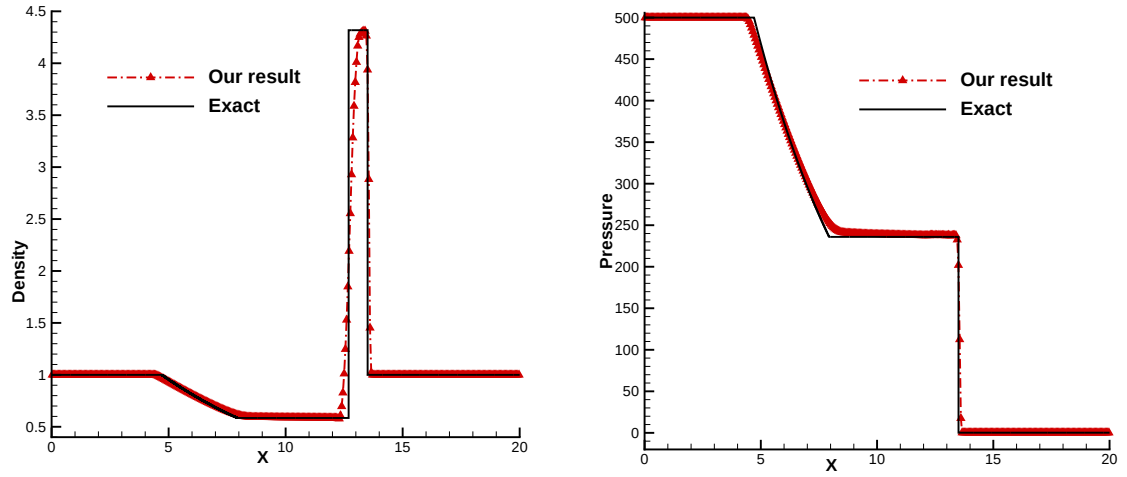

(a) Density (b) Pressure

Figure 3: The result of multi-material shock tube problem.

3.2.2 A multi-material Sod's shock tube problem

This example is a multi-material Sod's shock tube problem [10, 24]. In this test, we will evaluate the ability to simulate multi-material flows and essentially non-oscillatory property of our scheme. The computational domain is set to $[0,1]$, the initial condition is

$$(\rho,u,p,\gamma)=\begin{cases}(1.0,0,2.0,2.0), & \text{if} \quad x\leq 0.5,\\ (0.125,0,0.1,1.4), & \text{otherwise},\end{cases}$$

and the final time is $t=0.2$.

Fig. 4 shows the distributions of density, pressure and volume-fraction obtained by our multi-material OFDG scheme with 100 cells, 200 cells and 400 cells, respectively. Through the comparison between the exact solution and our results, we can see that our numerical solutions toward the exact one have good convergence as the number of cells increases. In addition, the numerical solutions with essentially non-oscillatory property have sharp shock wave fronts.

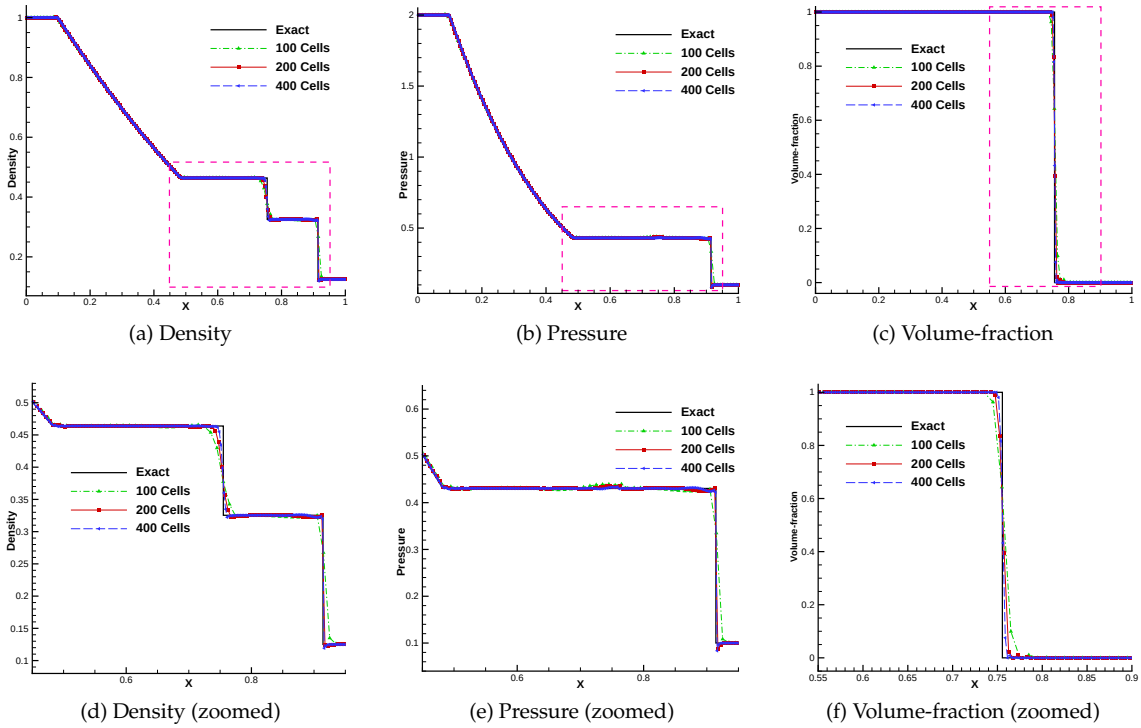

(a) Density (b) Pressure (c) Volume-fraction

(d) Density (zoomed) (e) Pressure (zoomed) (f) Volume-fraction (zoomed)

Figure 4: The distributions of density, pressure and volume-fraction of multi-material Sod's shock tube problem. Overall drawings (top); local zoomed-in drawings (bottom).

3.2.3 An air-helium shock tube problem

The final example for evaluating the ability to simulate the multi-material flows of our scheme is an air-helium shock tube problem. In this example, the computational domain is $[0,1]$, the initial condition of this case is as follows:

$$(\rho,u,p,\gamma)=\begin{cases}(1.0,0,1.0,1.4), & \text{if} \quad x\leq 0.5,\\ (0.125,0,0.1,1.667), & \text{otherwise},\end{cases}$$

and the final time is $t=0.2$. Fig. 5 shows the distributions of density and pressure with 200 cells. Compared to the exact solution, we can see that our algorithm gives acceptable numerical result except that there are a few very slight oscillations in certain areas. We think the reason for the slight oscillations is as follows. The damping terms described in this paper can perfectly handle general discontinuity problems. But for very strong shock wave problems, the viscosity introduced by the present damping terms may be insufficient, failing to achieve the perfect suppression of oscillations. In the future work, we will further investigate the improvement of damping terms for strong shock wave problems, so that this OFDG scheme can perfectly suppress the false oscillations in the strong shock wave problems and then enhances its applicability to various multi-material discontinuity problems.

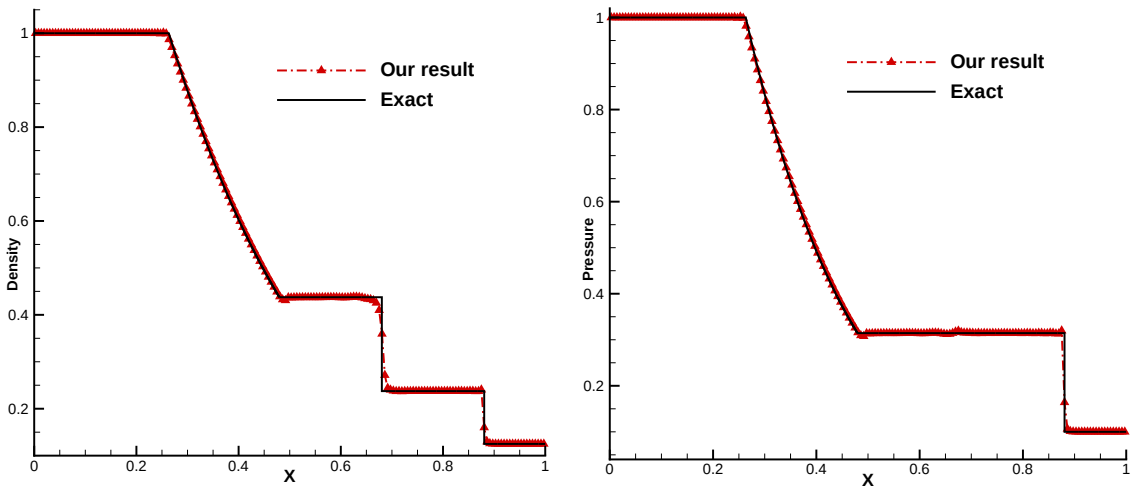

(a) Density (b) Pressure

Figure 5: The result of air-helium shock tube problem.

4 Conclusions

In this paper, we have shown a concise oscillation-free DG scheme for one-dimensional compressible multi-material flows. Without the classical slope limiters, our scheme introduced the new damping terms based on the jumps of variables at the cell boundary for controlling the numerical oscillations. The added damping terms do not involve the problem-dependent parameters, and they can adaptively detect the intensity of discontinuity and adjust their values according to the jumps of variables. Several examples are used for demonstrating the accuracy and essentially non-oscillatory property of our scheme. However, the current scheme still appears to suffer from a severe CFL restriction due to the explicit treatment highly stiff damping terms which act as an additional artificial viscosity. In addition, the scheme also suffers from the reliance on characteristic decomposition in the construction of damping coefficients. In the further work, we will study the higher-order OFDG scheme and extend our scheme into the simulation of higher-dimensional problems and more general equations of state. Notably, the situations of multi-dimensional problem with more general equations of state are even more complex than the ones of one-dimensional ideal gases. The specific challenge that the future work may face is how to choose an appropriate structure of the damping term to ensure the good non-oscillatory effect while avoiding introducing excessive numerical dissipation. The preliminary planned strategies for constructing the appropriate damping term are adjusting the coefficients and jump values in the damping term based on the numerical results of different examples. Furthermore, as a possible direction for future improvement, we will consider the oscillation-eliminating discontinuous Galerkin (OEDG) framework [17] to enhance efficiency and potentially relax time step restrictions. The strategies for improving the present scheme include applying the damping (oscillation-eliminating) step sequentially after each Runge-Kutta stage (operator splitting) to mitigate the time-step limitations and constructing damping coefficients based on wave-speed information for reducing the dependence on characteristic decomposition and so on.

Acknowledgments

This work is supported by the National Natural Science Foundation of China (Grant Nos. 12501572, 12501544), by the China Postdoctoral Science Foundation (Grant No. 2023M743212), by the Youth Foundation of National Key Laboratory of Computational Physics (Grant No. 6142A05QN24014) and by the Nat-

ural Science Youth Foundation of Henan Province (Grant Nos. 242300420625, 262300420327).

Author Contributions

All authors contributed to the study conception and design. Material preparation, data collection and analysis were performed by Xiaolong Zhao, Xiangyuan Li, Xijun Yu, Fang Qing and Zhenzhen Li. The first draft of the manuscript was written by Xiangyuan Li and Xiaolong Zhao, and all authors commented on previous versions of the manuscript. All authors read and approved the final manuscript.

References

[1] R. Abgrall, *How to prevent oscillations in multicomponent flow calculations: A quasi conservative approach,* J. Comput. Phys. 125 (1996), 150–160.

[2] R. Abgrall and R. Saurel, *Computations of compressible multifluids,* J. Comput. Phys. 169 (2001), 594–623.

[3] R. Abgrall and R. Saurel, *Discrete equations for physical and numerical compressible multiphase mixtures,* J. Comput. Phys. 186 (2003), 361–396.

[4] G. Allaire, S. Clerc, and S. Kokh, *A five-equation model for the simulation of interfaces between compressible fluids,* J. Comput. Phys. 181 (2002), 577–616.

[5] W. Boscheri, M. Dumbser, and E. Gaburro, *Continuous finite element subgrid basis functions for discontinuous Galerkin schemes on unstructured polygonal Voronoi meshes,* Commun. Comput. Phys. 32 (2022), 259–298.

[6] J. Cheng and C. Shu, *A high-order ENO conservative Lagrangian type scheme for the compressible Euler equation,* J. Comput. Phys. 227 (2007), 1567–1596.

[7] B. Cockburn and C. Shu, *The Runge-Kutta discontinuous Galerkin method for conservation laws II: General framework,* Math. Comp. 52 (1989), 411–435.

[8] B. Cockburn and C. Shu, *The Runge-Kutta discontinuous Galerkin method for conservation laws V: Multidimensional systems,* J. Comput. Phys. 141 (1998), 199–224.

[9] J. Du, Y. Liu, and Y. Yang, *An oscillation-free bound-preserving discontinuous Galerkin method for multi-component chemically reacting flows,* J. Sci. Comput. 95 (2023), Paper No. 90.

[10] S. Galera, P. H. Maire, and J. Breil, *A two-dimensional unstructured cell-centered multimaterial ALE scheme using VOF interface reconstruction,* J. Comput. Phys. 229 (2010), 5755–5787.

[11] A. Hiltebrand and S. Mishra, *Entropy stable shock capturing space time discontinuous Galerkin schemes for systems of conservation laws,* Numer. Math. 126 (2014), 103–151.

[12] S. Karni, *Multicomponent flow calculations by a consistent primitive algorithm,* J. Comput. Phys. 112 (1994), 31–43.
[13] S. Karni, *Hybrid multifluid algorithms,* SIAM J. Sci. Comput. 17 (1996), 1019–1039.
[14] Z. Li, X. Yu, J. Zhu, and Z. Jia, *A Runge Kutta discontinuous Galerkin method for Lagrangian compressible Euler equations in two-dimensions,* Commun. Comput. Phys. 15 (2014), 1184–1206.
[15] Y. Liu, J. Lu, and C. Shu, *An essentially oscillation-free discontinuous Galerkin method for hyperbolic systems,* SIAM J. Sci. Comput. 44 (2022), 230–259.
[16] J. Lu, Y. Liu, and C. Shu, *An oscillation-free discontinuous Galerkin method for scalar hyperbolic conservation laws,* SIAM J. Numer. Anal. 59 (2021), 1299–1324.
[17] M. Peng, Z. Sun, and K. Wu, *OEDG: Oscillation-eliminating discontinuous Galerkin method for hyperbolic conservation laws,* Math. Comp. 94 (2025), 1147–1198.
[18] J. Qiu and C. Shu, *Runge-Kutta discontinuous Galerkin method using WENO limiters,* SIAM J. Sci. Comput. 26 (2005), 907–929.
[19] K. M. Shyue, *An efficient shock-capturing algorithm for compressible multicomponent problems,* J. Comput. Phys. 142 (1998), 208–242.
[20] Q. Tao, Y. Liu, Y. Jiang, and J. Lu, *An oscillation free local discontinuous Galerkin method for nonlinear degenerate parabolic equations,* Numer. Methods Partial Differential Equations 39 (2023), 3145–3169.
[21] P. Woodward and P. Colella, *The numerical simulation of two dimensional fluids with strong shock,* J. Comput. Phys. 54 (1984), 115–173.
[22] F. Zhang and T. Liu, *A high-order direct discontinuous Galerkin method for variable density incompressible flows,* Commun. Comput. Phys. 32 (2022), 850–877.
[23] W. Zhang, Y. Xing, Y. Xia, and Y. Xu, *High-order positivity-preserving well-balanced discontinuous Galerkin methods for Euler equations with gravitation on unstructured meshes,* Commun. Comput. Phys. 31 (2022), 771–815.
[24] X. Zhao, X. Yu, M. Qiu, F. Qing, and S. Zou, *An arbitrary Lagrangian-Eulerian RKDG method for multi-material flows on adaptive unstructured meshes,* Comput. Fluids 207 (2020), Paper No. 104589.
[25] H. Zheng, C. Shu, Y. Chew, and N. Qin, *A solution adaptive simulation of compressible multi-fluid flows with general equation of state,* Internat. J. Numer. Methods Fluids 67 (2011), 616–637.
[26] J. Zhu, X. Zhong, C. Shu, and J. Qiu, *Runge-Kutta discontinuous Galerkin method using a new type of WENO limiters on unstructured meshes,* J. Comput. Phys. 248 (2009), 200–220.
[27] H. Zuo, W. Zhao, and P. Lin, *An oscillation-free bound-preserving discontinuous Galerkin method for multi-component chemically reacting flows,* J. Comput. Phys. 505 (2024), Paper No. 112906.
[28] H. Zuo, W. Zhao, and P. Lin, *The jump filter in the discontinuous Galerkin method for hyperbolic conservation laws,* J. Comput. Phys. 520 (2025), Paper No. 113498.